SEDIMENTOLOGY the journal of the International Association of Sedimentologists

Sedimentology (2022) doi: 10.1111/sed.12974

The stratigraphic significance of self-organization: Exploring how autogenic processes can generate cyclical carbonate platform strata

HAIWEI XI and PETER M. BURGESS
Department of Earth, Ocean and Ecological Science, Quantitative Experimental Stratigraphy Group, Jane Herdman Laboratory, University of Liverpool, Brownlow Street, Liverpool L69 3GP, UK (E-mail: Haiwei.Xi@liverpool.ac.uk)

Associate Editor – Hairuo Qing

ABSTRACT

Autogenic spatial self-organization can produce coherent patterns of ordered cyclical strata through interaction of system components, independent of initial conditions and without external forcing. Previous numerical modelling work that partially explored self-organized cyclicity in carbonate strata is expanded, refined and tested using a different numerical model formulation of an existing carbonate forward model 'CarboCAT'. Results show that cross-platform sediment transport creates a series of self-organized prograding islands and shorelines that generate upward-shallowing autocycles, defined by strong statistical evidence for ordered facies successions. A subtidal factory in front of each shoreline supplies sediment that drives shoreline progradation and these subtidal supply-zone widths are also self-organized to an optimal characteristic width due to island progradation, such that an accommodation creation/sediment supply ratio of around one maintains self-organized shoreline progradation. The resulting island progradation rate determines autocycle thickness, which is very different from the accommodation control assumed in most sequence stratigraphic and cyclostratigraphic interpretations. This self-organization process is comparable to the reaction–diffusion model first suggested by Alan Turing. The simplest possible combination of processes that leads to self-organization are water-depth-dependent production, straight long-distance cross-platform transport and uniform subsidence. Additional more complex processes can produce self-organization, but also more diverse island morphologies, less ordered autocyclic strata and more variable lateral facies continuity. Exploration of the model parameter space shows that self-organization occurs for only a limited range of accommodation creation/sediment supply ratios. The modelling is calibrated and checked for realism against shoreline progradation rates measured on the Peros Banhos carbonate platform, British Indian Ocean Territory, and a Holocene Abu Dhabi shoreline, suggesting that this is a realistic and perhaps ubiquitous process in geological history. Given the fundamental nature of processes modelled here, and the match with observed processes in modern depositional systems, it seems possible that similar autogenic, self-organizing processes have operated on many carbonate platforms and are an important component in the stratigraphic record.

Keywords Autogenic, carbonate platform, numerical model, sedimentary record, spatial self-organization.

INTRODUCTION

Carbonate strata are frequently interpreted to be cyclical on a scale of a metre to a few metres (Read *et al.*, 1986; Goldhammer *et al.*, 1987, 1990; Enos, 1991; Osleger & Read, 1991; Christ *et al.*, 2012), although the evidence for such interpretation is often too weak to robustly support this interpretation (Drummond & Wilkinson, 1993; Wilkinson *et al.*, 1997; Burgess, 2016). The cyclicity is most often assumed to be forced by external factors, such as eustasy or tectonic pulses (Goldhammer *et al.*, 1987, 1990; Chen *et al.*, 2001; Bosence *et al.*, 2009), but also sometimes ascribed to autocyclic processes (Goldhammer *et al.*, 1993; Lehrmann & Goldhammer, 1999; Burgess, 2001). Ginsburg (1971) suggested that metre-scale peritidal parasequences can be generated by long-term uniform subsidence, landward movement of carbonate muds, progradation of a shoreline over the subtidal mud factory, followed by progressively reduced production and sediment supply and transgressive flooding, all based on observation from Florida Bay lagoon and tidal flats of the Bahamas. These cycles are referred to as 'autocycles' due to their autogenic origin alone with an absence of any external forcing. A slightly more complex tidal flat island model is proposed by Pratt & James (1986) that involves complex shoal and tidal flat island migration through time, which can produce a shallowing-upward parasequence in any given vertical section at the platform interior. In their model, tidal flat islands evolved with changing regional hydrographic conditions and the distribution of sediment types around these islands varied spatially and temporally, due to localized responses to local sediment supply on the evolving seafloor. Both of these models require some spatial feedbacks in the depositional system for the processes to operate in a predictable way, and therefore suggest the possibility of a self-organizing process driving formation of autocycles.

Spatial self-organization is a process in which a coherent pattern emerges through interaction of system components. Self-organization processes are pervasive and widely documented across many natural systems (Rietkerk & Koppel, 2008; Hajek *et al.*, 2010; Paola, 2016), with conceptual origins in classic 'chemical reaction–diffusion' theory (Turing, 1952). In this reaction–diffusion process, local feedbacks occur between reaction components, but spatial information is also transmitted over a longer distance via diffusion as individual particles migrate across a volume. Levin & Segel (1985) extended this theory to understand ecological diversity and heterogeneity, in which reaction is generalized to local interaction, and diffusion is replaced by more general longer distance transport mechanisms. Self-organization in these cases can explain the striking spatial patterns observed at various levels in biological systems that are spatially complex and heterogeneous yet have a degree of regularity or coherency. Emergence and maintenance of these spatial patterns from an initial uniform or disordered state, all by undirected local interaction of system components and global redistribution, is generally referred to as 'spatial self-organization'.

Pattern formation is one of the most prominent characteristics of spatial self-organization, and this process can be spontaneous if sufficient energy is available in the system. Self-organized patterns are often easily identifiable, persistent and predictable across a range of scales (Purkis *et al.*, 2016b). In ecological systems, these coherent patterns are banded, striped or labyrinthine, and usually lead to resource optimization increasing overall productivity and diversity of the system (von Hardenberg *et al.*, 2001; Thar & Kühl, 2005). Interactions are local phenomena, but spatially self-organizing systems also typically feature system-wide redistribution of material that creates order and pattern as the system approaches a state of dynamic equilibrium. This equilibrium state is maintained by both scale-dependent positive and negative spatial feedbacks (Levin & Segel, 1985; Budd *et al.*, 2016) with development of some robust structures to weaken or even negate perturbation effects from external environmental changes (Liu *et al.*, 2013). A wide range of examples of spatial self-organization in modern sedimentary systems have been recognized and discussed, including formation of bedforms (Fedele *et al.*, 2016), evolution of channels and fans in fluvial-deltaic systems (Paola *et al.*, 2009; Kim *et al.*, 2014; Paola, 2016), morphodynamics of aeolian dune field (Kocurek & Ewing, 2016) and ecological succession (Olszewski, 2016). In carbonate depositional systems, spatial self-organization seems likely to have an important role in controlling the spatial structure and expression of the whole system, by generating different patterns across a wide range of scales, supported by studies of hot spring microbial carbonates (Petroff *et al.*, 2010), modern bivalve beds (Rietkerk & Koppel, 2008), and formation of patterned coral reefs

and tidal channel systems (Fagherazzi, 2008; Purkis *et al.*, 2016b).

Despite the abundance of contemporary examples, the potential influence of spatial self-organization on ancient strata from carbonate depositional systems is still generally poorly understood and poorly documented compared to interpretations of allocyclic forcing, with a few notable exceptions. Previous numerical modelling by Drummond & Dugan (1999) attributes negative exponential bed thickness-frequency distribution and log-log linear forms of area-frequency distribution in strata to aspects of self-organization. Quantitative analysis of north-west Andros Island suggests that subfacies area, distance and lateral facies transitions are highly ordered, probably due to self-organization (Rankey, 2002). Forward modelling of peritidal carbonate systems suggests that the 'Ginsburg-type' shoreline progradation process is self-organizing, producing coherent planform patterns and cyclic vertical sections (Burgess *et al.*, 2001; Burgess & Wright, 2003). Better understanding and documentation of spatial self-organization for producing autogenic stratal order and cyclicity is particularly important given that these attributes of strata are so often interpreted, often with insufficient evidence, to be due to other more allogenic processes.

The aim of this paper is to demonstrate, explore more fully and discuss how carbonate autocycles can be understood as a product of self-organizing processes of sediment production and sediment transport on carbonate platform tops, building on previous work that suggested this as a possibility (Burgess *et al.*, 2001; Burgess, 2006) but did not explore in detail how the self-organizing processes worked, or the full implications for development of cyclical strata. Better understanding of the likely links between spatial self-organization and autogenic dynamics could significantly enhance interpretation and prediction of the record of Earth history in carbonate strata, as well as helping in predictions for the likely response of modern carbonate platforms to current rapid climate change.

MODEL FORMULATION

Model description

'CarboCAT' is a reduced-complexity numerical forward model designed to explore the evolution of carbonate platforms and the strata they produce. The model is documented in detail in Burgess (2013) and Masiero *et al.* (2020). This current study uses a new version of CarboCAT modified to include elements from Burgess *et al.* (2001) and Burgess & Wright (2003), to explore and understand how cross-platform sediment transport can produce self-organized autocyclic carbonate strata. All of the model runs presented here have a 1 kyr duration time step, so the calculation of sediment transport for each time step is a simplified representation of long-term cross-platform unidirectional sediment transport due to the time-averaged effects of waves and currents. Sediment transport follows either a straight line in an onshore direction from entrainment in the seaward subtidal area to deposition in the landward intertidal area (for example, model Case 2 and Case 3), or a more complex onshore route, influenced by variations in platform top bathymetry following simple rules of refraction of transport direction in shallow water (model Cases 4 to 9).

Modified CarboCAT uses a simple orthogonal regular model grid consisting of 100 data points in the dip direction and 30 data points along the strike. Model grid point spacing is 200 m, so the total grid represents a 20×6 km surface. Each time step represents one thousand years, and a total of 2000 time steps in all model runs shown here gives a total elapsed model time (EMT) of 2 Myr. Elevation and water depth values are stored at every grid point in the model and calculated then updated each time step by subsidence, *in situ* production of particular facies, and sediment transport. Tidal currents are not modelled explicitly, but a tidal range of 1 m is assumed in the classification of peritidal strata, such that strata deposited with water depth of <1 m are classified as intertidal, and strata deposited above sea-level are supratidal.

A uniform subsidence rate is applied across the entire model grid. Each cell can either contain a single *in situ* carbonate facies or be empty, and the spatial distribution of facies and empty cells is determined by cellular automata rules, simulating facies dynamics in response to ecological stress (Burgess, 2013). Autotrophic organisms require light for photosynthesis, so modelled carbonate production rate decreases with increasing water depth as an approximation of decreasing light penetration into deep water (Bosscher & Schlager, 1992), and modified by a scaling factor R (Masiero *et al.*, 2020). The value of R is calculated from the cellular automaton, producing a symmetrical profile

showing increased production due to resource optimization and colonization, followed by a linear decrease due to competition of space and nutrients (Fig. 1A). *In situ* carbonate production is cut off in water depth less than 1 m to represent reduced carbonate production in the intertidal zone where subaerial exposure is frequent.

Sediment transport rate is determined by the fraction of *in situ* production available for transport, which is a constant for each facies, and a representation of water flux over the grid cell. As in previous models (Burgess *et al.*, 2001), onshore prevailing winds and currents are assumed to produce a time-averaged net onshore advective sediment flux. Magnitude of this sediment flux is assumed to be proportional to wave amplitude and wavelength, and to current velocity. Flowing water entrains sediment if the sum of slope shear stress and shear stress induced by flowing water is greater than a user-specified threshold, using equation (20) from Warrlich *et al.* (2002). This threshold is a function of grain size, so a higher value represents coarse-grained sediment, and a lower value represents fine-grained sediment.

If sediment is removed and entrained, it can be transported either in a straight line towards the landward edge of the model grid, or along a more complex landward route modified locally due to interactions with topography in shallow water, calculated cell-by-cell using Snell's Law (Martinez & Harbaugh, 1989). For each cell on the model grid, current velocity (vel) can be calculated from input wavelength (λ) and water depth (wd) such that.

$$\mathrm{vel}(i,j) = \sqrt{\frac{\lambda * g}{2\pi}} * \tanh\left(\frac{2\pi}{\lambda} * \mathrm{wd}(i,j)\right) \quad (1)$$

Transport direction (θ_{wave}) between cell (x, y) and the next more landward cell (x, $y+1$) is calculated by averaging the two relative transport directions in adjacent cells (θ_B and θ_C) and scaling by a parameter that determines the degree of water depth and topographic influence on the flow direction (F) (Fig. 1B):

$$\theta_B = \alpha + \frac{\arctan(\mathrm{vel}(x-1,y) - \mathrm{vel}(x,y))}{F} \quad (2)$$

$$\theta_C = \alpha + \frac{\arctan(\mathrm{vel}(x,y) - \mathrm{vel}(x+1,y))}{F} \quad (3)$$

$$\theta_{\mathrm{wave}} = \frac{\theta_B + \theta_C}{2} \quad (4)$$

Therefore, a low value of F means the transport is very sensitive to topography and will diverge markedly from an onshore direction when influenced by changes in water depth, such that flows tend to converge towards areas of shallow water depth and deposit sediments (Fig. 1B), leading to deposition of the sediment over a wider section of the landward shoreline. In contrast, when F is high, sensitivity to topography is much lower, and deviations from landward transport are much smaller. This new formulation of CarboCAT also contains a stochastic element that allows, in rare cases, transport into and deposition in cells where water depth is less than zero. By defining a probability

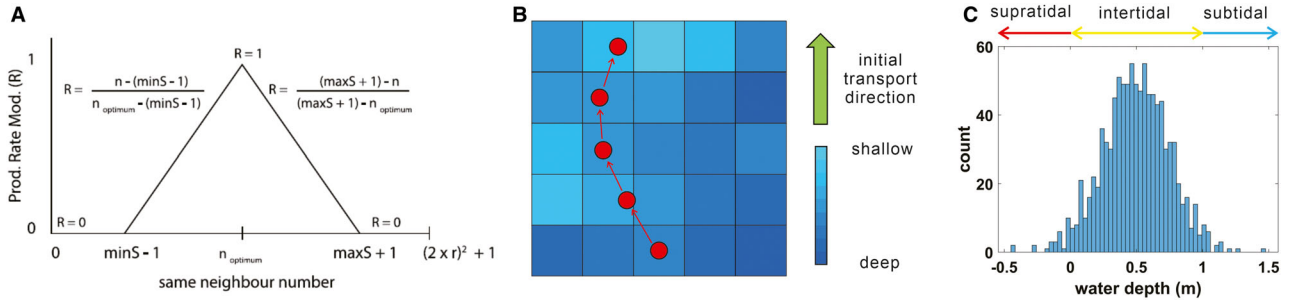

Fig. 1. (A) Production rate modifier (R) rationale in CarboCAT. R is equal to one (maximum carbonate production) in model cells with the optimum number of same-facies neighbours (*noptimum*). R decreases linearly from one to zero where the number of same-facies cells is equal to *minS* or *maxS* and the resulting carbonate production is zero, from Masiero *et al.*, (2020). (B) Rationale of topography-controlled sediment transport, red arrow indicates flow pathway, flows will converge towards shallow water depth area following Snell's law. (C) Probability distribution of depositional water depth, majority of the depositional events are still within the intertidal zone, with occasional depositional events on supratidal by large storm events.

distribution of this happening, the probability of supratidal deposition is low, and most of the transported sediment is still deposited in the intertidal zone (Fig. 1C), so the stochastic supratidal depositional events are analogous to large storm events that might occur within the duration of a single time step. The supratidal deposition is important to amalgamate layers and increase lateral facies continuity (Olivito & Souza, 2020).

As well as longer distance onshore sediment transport, short-distance downslope sediment transport off local topographic highs into surrounding depressions is also modelled. Local transport is calculated using a diffusion law, smoothing the topography at rates dependent on local slope and a diffusion coefficient. It is calculated using a simple implicit Crank-Nicholson finite-difference solution (Crank, 1975).

Model cases: Input parameters and modelled processes

To understand the role of self-organization in this model behaviour, this study first demonstrates a non-self-organized case which generates a carbonate platform without autocycles. Model elements are then progressively added to run eight additional models (Table 1), to understand how each element contributes to the emergence of self-organization and autocycle formation. Input parameters are based on reasonable, constrained values used in previous studies of peritidal carbonate systems (Kenyon & Turcotte, 1985; Enos, 1991; Bosscher & Schlager, 1992; Burgess & Wright, 2003). Initial model topography is always low-angle ramp, with a zero-flux subaerial barrier on the landward edge of the model grid. Transport fraction is set to 0.5, which means up to half of the *in situ* production is available for transport in the flat-top platform setting. The diffusion coefficient of 20 000 m^2 per year is consistent with other estimates for shallow water diffusional transport (Kaufman *et al.*, 1991; Williams *et al.*, 2011).

RESULTS

Case 1: Progradational platform, disorganized shorelines, no autocycles

Case 1 shows a typical evolution of carbonate platform from a ramp to a flat-topped platform but without formation of prograding coherent islands and autocycles. Production occurs across the whole model grid initially, but later in the model run is restricted to the platform top as

Table 1. Input parameters and statistic metric of total nine model runs.

Case	1	2	3	4	5	6	7	8	9
Subsidence	50								
Production rate	200	70	200						
Cellular automata	On	Off	On						
Transport	Downslope	Straight Onshore	Straight Onshore	Wave refraction F = 1	Wave refraction F = 5	Wave refraction F = 25	Wave refraction F = 5	Wave refraction F = 5	Wave refraction F = 5
Diffusion	Off	Off	Off	Off	Off	Off	K = 20 000	K = 100 000	K = 500 000
Spatial entropy	0.075846	0.1370	0.064895	0.067156	0.08168	0.09254	0.19136	0.19346	0.2154
Stratigraphic completeness	0.2965	0.5012	0.2157	0.2611	0.2655	0.2651	0.3991	0.4451	0.5542

Spatial entropy indicates the lateral heterogeneity and stratigraphic completeness is the proportion of elapsed model time recorded by strata accumulation; but neither of them here can clearly distinguish the disordered Case 1 from the semi-ordered Case 9 and the remaining seven ordered cases.

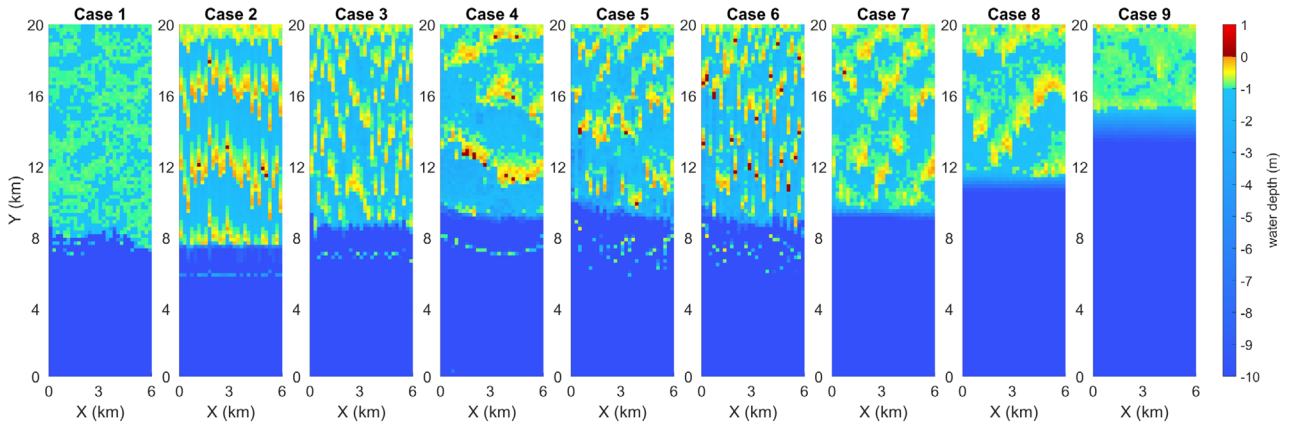

Fig. 2. Map view of platform tops at 2 Myr elapsed model time for all model cases. Case 1 has downslope sediment transport, and it does not have any onshore sediment flux for island progradation. Instead, it shows a wide low-relief tidal flat without any identifiable patterns. Case 2 has simplest model formulation and islands prograde and self-organize into sinuous belts with equal subtidal zones spacing between islands. Islands slightly break up in Case 3 due to spatially-complex production in the subtidal zone. Cases 4 to 6 all show coherent patterns, but with variations in island morphology, lateral continuity and spatial distribution. Implementing diffusional transport in Case 7 can increase the island area and reduce island irregularity compared to Case 5. But as diffusion coefficient becomes very high in Case 9, islands are eliminated and cannot act as effective barriers to sediment transport, the self-organizing interactions between production, transport and subsidence are disrupted, so the islands and subtidal zones are arranged without any coherency.

water depths off the platform increase. Sediments are transported downslope locally where the surface gradient exceeds a transport threshold. The platform interior is an irregular mosaic of subtidal and intertidal deposition due to local variations in production rate and downslope sediment transport (Case 1; Fig. 2). There is no onshore sediment flux to create and prograde shorelines and islands, and in the absence of any external forcing also, the platform interior strata are disordered and lack spatial patterns (Fig. 3).

Cases 2 and 3: Minimum processes required to generate shoreline progradation and autocycles

In model Case 2 and Case 3, sediment is transported landward in a straight line until deposition occurs in front of the subaerial barrier. Initially this occurs at the model grid boundary and generates a supratidal shoreline and intertidal bank along the proximal edge of the model grid (Fig. 4). Continued transport accretes sediments on the windward side of this shoreline, which then progrades when the accommodation–supply ratio (A/S) is less than one along the front of the island. The leeward side of the island is sediment starved, subsides back into subtidal zone and floods, so the shoreline becomes a detached, prograding island barrier (Fig. 4) (see also descriptions in Burgess *et al.*, 2001), rather than an attached shoreline as in Ginsburg's model (Ginsburg, 1971). Prograding islands in Case 2 are slightly sinuous and approximately equally-spaced, separated by wide subtidal zones that supply sediment to be transported and accreted onto the shoreline. The widths of subtidal sediment-production zones in Case 3 are more variable, because of the spatially-variable production rates in the model (Fig. 2; Table 1). As the island migrates seaward, a new subtidal zone develops landward which feeds sediment further landward. Once it is wide enough to produce sufficient sediment, this creates another prograding shoreline, and the process repeats to generate multiple cycles in strata (Fig. 4). The first cycle emerges in less than 0.1 Myr, and island migration across the platform top generates more than 20 cycles of shallowing-upward strata in vertical section in a time span of 2 Myr (Fig. 3). This is similar to the process of shoreline and island progradation first proposed by Ginsburg (1971) and later explored in numerical models (Goldhammer *et al.*, 1993; Burgess *et al.*, 2001; Burgess & Wright, 2003).

Because the platform top operates in keep-up mode, water depth in the subtidal zone is

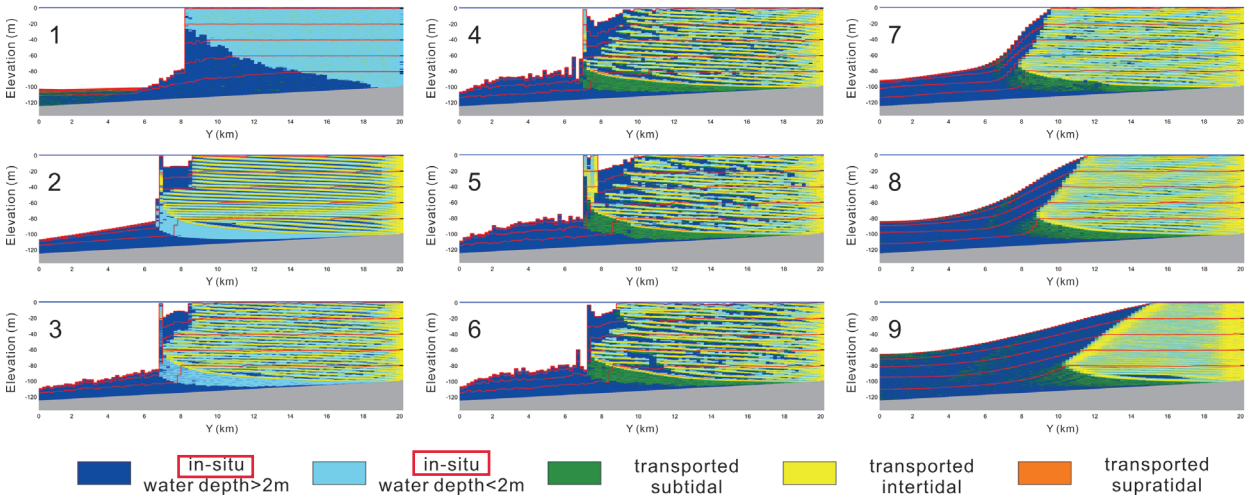

Fig. 3. Cross-section of all model cases at $x = 3$ km. Platform margin position, platform interior lateral facies continuity and relative proportion of each facies vary between models due to different input parameters and model processes (Table 1) but all the models except Case 1 and Case 9 show strong apparently cyclical layering in the platform interior arising from progradation of islands due to onshore sediment transport. The cyclic facies arrangement in vertical sections are results of their varying degree of order and pattern in planform the islands show as in Fig. 2. Note that the distal end of the model is too deep for *in situ* production after about 1 Myr, so platform margins retreat due to insufficient sediment flux in Case 2 to Case 9. Only the downslope transported-dominated Case 1 can maintain progradation without this issue. Red lines represent timelines at every 0.4 Myr.

generally shallow, in the order of 1 to 2 m. This means magnitude of sediment supply to the windward shoreline of each island is determined by the width of the adjacent more distal subtidal factory. If sediment supply to the shoreline is greater than the rate of accommodation creation at the shoreline (A/S < 1), shoreline progradation occurs. Increased sediment transport rate at particular subsidence and production rates will decrease the subtidal area width, and the subtidal area width in turn determines the thickness of the autocycles produced by the progradation process (Burgess *et al.*, 2001). These observations of model behaviour are very important, for two reasons. Firstly, the relationship between width of the subtidal zone, sediment supply to the shoreline and shoreline progradation, is an example of a spatial feedback where, for any given rates of sediment production and sediment transport, subtidal zone width determines the shoreline progradation rate and shoreline progradation rate in turn determines the subtidal zone width. Secondly, it means that autocycle thickness in these cases is controlled by the A/S ratio at each prograding island shoreline, and there is no requirement for external forcing to produce ordered, cyclical strata. This does not exclude the possibility of external forcing to produce similar cycles in outcrops but suggests an equally plausible autogenic explanation, or perhaps a mix of both processes. Case 2 and Case 3 demonstrate that subsidence, *in situ* depth-dependent sediment production, and landward cross-platform sediment transport perpendicular to the shoreline, with spatial feedbacks operating between these processes, are the simplest combination of numerical model components that can generate autocycles.

Cases 4 to 6: Effects of transport direction controlled by topography

When comparing the platform top map view of Case 4 with Case 3 (Fig. 2), increased sensitivity of sediment transport direction to topography clearly increases lateral island continuity, which suppresses the spatial variability of production in subtidal zone. Low values of the flow-topography relationship parameter F (for example, Case 4; Fig. 2) makes sediment transport more sensitive to water depth variation on the transport pathway, which may then diverge markedly from the prevailing wind direction. A consequence of this divergence is that any given volume of sediment will be redistributed to a wider portion of shoreline; hence each shoreline

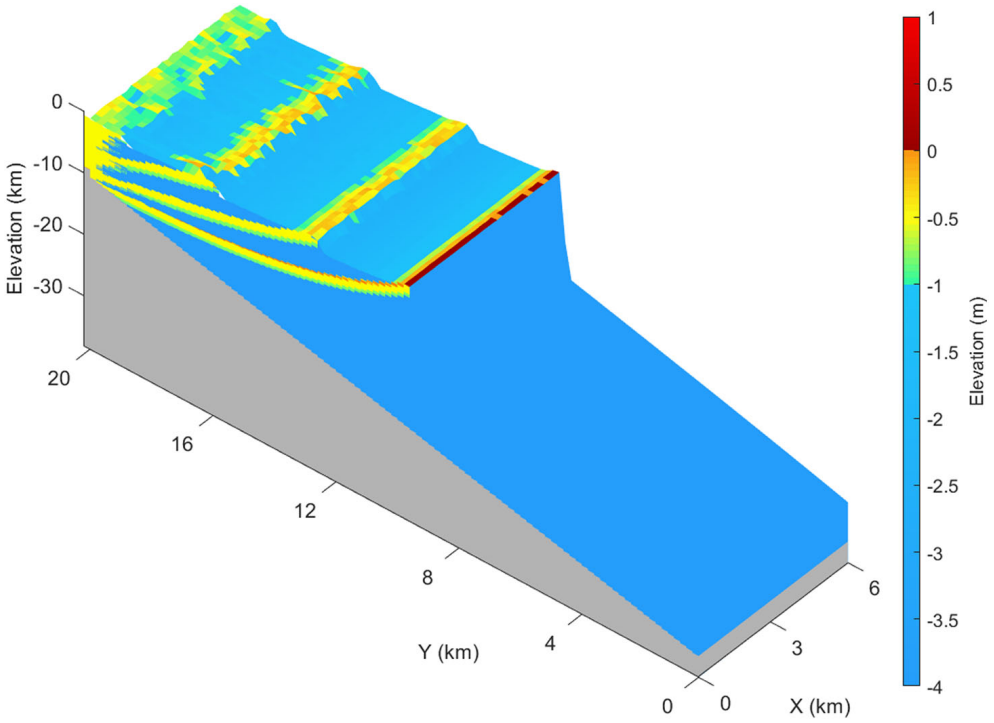

Fig. 4. Three-dimensional block diagram of model Case 2 at 0.2 Myr, which shows the self-organizing interactions between uniform subsidence, *in situ* production and onshore sediment transport. Islands are arranged in linear belts with very wide subtidal zones in between to supply sufficient sediments to the adjacent island by long-distance cross-platform transport, which produce island progradation as A/S ratio <1. Island progradation is planform leads to shallowing-upward autocyclic parasequences.

point will tend to receive less sediment on average so the difference between adjacent cells will be reduced. This helps to reduce variations of progradation rates along strike, prevents island break-up, and generates more regular and rounded island shapes with well-defined edges (Case 4; Fig. 2).

Increasing the flow-topography relationship parameter F has the opposite effect. The spatial variations of production in the subtidal zone leads to differential lateral accretion rates on the windward side of islands which consequently prograde at different rates and eventually break up (Case 6; Fig. 2). Since the fundamental subsidence, production and transport rates are unchanged in Cases 4 to 6, the subtidal zone width and island width are similar in these three cases (Fig. 5B). Comparing Case 2 with Cases 3 to 5, the more complex sediment transport pathways in later cases cause different topographic expressions and morphodynamics, which produce more complex three-dimensional connectivity with reduction of lateral facies continuity (Fig. 3).

Cases 7 to 9: Effect of local downslope diffusional transport

Diffusional transport in this model is a short-distance smoothing process, relative to the longer-distance advective cross-platform transport. Local diffusional transport tends to redistribute supratidal and intertidal sediment to adjacent subtidal lows. Comparing platform-top maps in Case 5 and Case 7 (Fig. 2), which are identical except for operation of diffusion in Case 7, shows that diffusional transport creates more rounded island morphology by suppressing the effects of lateral differential progradation demonstrated in Case 4. It can also coalesce separated islands and increase lateral facies continuities in cross-section by filling the subtidal zone in between (Fig. 3). These effects are also present in Case 8 with a higher diffusion coefficient K.

However, in Case 9, when K is further increased, diffusion can decrease the influence of island topography as effective 'barriers' to sediment transport. Without intertidal and

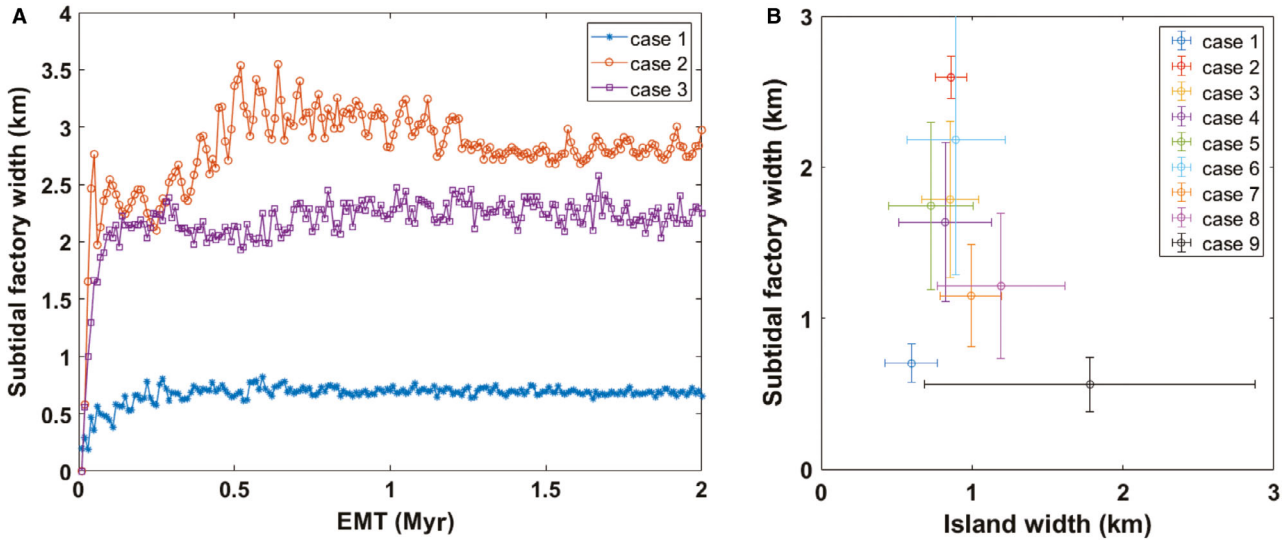

Fig. 5. (A) Time evolution of mean subtidal factory width for Cases 1, 2 and 3, showing different widths at dynamic equilibrium state, as seen in previous platform top maps and cross-sections. Attainment and maintenance of this state suggest that as shorelines and islands prograde, they organize to form a dynamic equilibrium planform island spacing characteristic for the particular subsidence, production and transport rate on the platform top. (B) Cross-plot of mean subtidal width against island width for all nine model cases. Error bars represent calculated standard deviation at 2 Myr. Case 2 has highest mean subtidal zone width and lowest standard deviation (see also Fig. 4). Note that Cases 2 to 8 show coherent patterns on platform top, and cyclic strata in vertical section, and all have subtidal widths >1 km, suggesting that a subtidal width >1 km indicates is associated with presence of self-organization.

supratidal island topographic barriers, the leeward side of islands can still receive sediments and does not subside back into the subtidal zone as in Cases 2 to 8. Consequently, in Case 9, islands expand laterally and amalgamate into an extensive low-relief intertidal flat, and subtidal factories become too narrow to produce and supply much sediment (Figs 2 and 5B). In this case, cross-platform sediment transport and island progradation are almost completely inhibited, and little self-organized pattern emerges (Fig. 3).

COMPARISON WITH TURING'S SELF-ORGANIZATION MODEL

It is suggested here that emergence of a patterned distribution of island and subtidal factory topography on the platform top in this model (Fig. 2), without any external forcing, is evidence of spatial self-organization. This self-organization is analogous to the classic 'reaction–diffusion' model of morphogenesis, first described by Turing (1952). In Turing's model, local feedbacks occur between reaction components, but spatial information is also transmitted over a longer distance via diffusion. Stable patterns or structures can develop due to the interaction between activator and inhibitor if the diffusion of inhibitor is faster than activator. So the activator will only spread locally because it cannot be produced and spread over longer distance (Turing, 1952). The net feedback is scale-dependent, such that positive feedback dominates at short scale, and negative feedback dominates at large scale.

In comparison with Turing's model, in this modified CarboCAT model, processes that maintain the influence of island topography as 'barriers' to shelter the leeward side, and reduce variations in island progradation rate along strike, such as topography-controlled sediment transport (Case 4), and local downslope diffusional transport (Case 7) are somewhat analogue to the 'activator' in the Turing model. By contrast, processes such as subsidence and very high-rate downslope sediment transport (Case 9) are 'inhibitors', because they tend to submerge or smooth island topography and therefore have system-wide negative effects on sediment production and transport to drive continuous progradation.

This comparison suggests that the modified CarboCAT model is recreating some key elements of the original Turing activator–inhibitor model and producing self-organized spatial patterns for somewhat similar reasons. However, in this model, processes and interactions seem to be more complex. For example, variable topographically-influenced sediment transport and diffusional transport, in Cases 4 to 9, have an important control on sediment redistribution and lead to very different island morphological development and stratigraphic expression depending on how they interact with other processes. It is also important to consider that the duration of a carbonate depositional system is several orders of magnitude higher than Turing's chemical experiments, and therefore more spatial and temporal variation of transport rate are likely to occur, also making this model more complex than the Turing model.

QUANTITATIVE EVIDENCE OF SPATIAL SELF-ORGANIZATION

Results from the nine model cases demonstrate how subsidence, sediment production and cross-platform sediment transport can produce emergent planform island and subtidal factory patterned morphologies. Cases 2 through to 8 show through visual examination elements of pattern that could be considered evidence for self-organization. However, quantitative evidence is required to properly demonstrate that self-organization is definitely present. The current study combines two different statistical methods to quantify the degree of order, and to measure the presence and evolution of self-organization in both planform (Fig. 2) and vertical succession (Fig. 3) patterns of strata.

Analysis of subtidal sediment factory width

Autocycle thickness and shoreline progradation rate in modelled cases are controlled by the A/S ratio and subtidal zone width at each prograding island shoreline. This A/S ratio requirement for progradation is a form of local feedback that is integral to the emergence of pattern in the model because, as shorelines and islands prograde, they organize to form a dynamic equilibrium planform island spacing characteristic for the particular subsidence, production and transport rate on the platform top (Fig. 5A). Attainment of dynamic equilibrium, with formation of distinct subtidal factories between intertidal and supratidal islands, leads to a form of resource optimization in the system, such that each subtidal carbonate factory can produce just enough sediment for island progradation. This can also be viewed as an emergent property internal to the system, the emergence and subsequent maintenance of this property is evidence of spatial self-organization occurring in the modelled system (Plotnick, 2016). In this model, Cases 2 to 8 all have mean subtidal factory width greater than 1 km, as subtidal factories become sufficiently unrestricted to produce and transport sediment to support a dynamic equilibrium state of island progradation, while subtidal widths in Case 1 and Case 9 are narrower and do not develop organized prograding islands (Fig. 5B). Based on this and supported by comparison of the appearance of island patterns in planform, it is suggested that model Cases 2 to 8 are potentially self-organized, while model Case 1 and Case 9 are not.

Analysis of facies and thickness order and cyclicity in vertical successions

In the absence of external forcing, presence of order and cyclicity in modelled vertical successions of strata requires an autocyclic process to form. The current model results show strong evidence for self-organization producing patterns in the planform arrangement of subtidal, intertidal and supratidal zones. Most interestingly, lateral migration of these planform patterns should, following Walther's Law, produce similarly ordered, autocyclic patterns in the vertical arrangement of subtidal, intertidal and supratidal facies. To test for these patterns, quantitative analysis of vertical sections can demonstrate which model cases show ordered strata, and which do not. If quantitative evidence indicates ordered vertical strata in model cases where spatial self-organization is present, and an absence of detectable order in the non-self-organized model cases, this suggests that, in this modelled system at least, there is a causal link between planform spatial self-organization and cyclical strata in vertical section.

For each of the nine model cases lithofacies and lithofacies unit thickness are analyzed from a vertical stratigraphic section taken from the centre of the model grid (y = 10 km, x = 3 km) using a facies transition probability and runs analysis method from Burgess (2016). A Markov metric m is calculated from a facies transition

probability matrix to characterize the vertical facies succession as a single value. This m value is then compared with m values calculated from disordered synthetic sections, generated by randomly shuffling the lithological units in the section. This is repeated 5000 times in a Monte Carlo process to generate a probability density function of m values. By comparing the calculated m value calculated from a modelled vertical section with the probability density functions arising from the randomly shuffled strata, a probability value p_m can be obtained and indicates the degree of order in the facies succession, with values close to zero indicating that the observed modelled succession was very unlikely to occur by chance (Burgess, 2016).

A similar approach is adopted for lithofacies unit thickness. A run is defined by Davis (2002) as an uninterrupted occurrence of a particular state within a series, for example a set of consistently thinning-upward units. The calculated runs order metric r quantifies the number and length of runs in a succession and allows a similar Monte Carlo approach to compare the r value from the observed section with a probability distribution function of equivalent but randomly shuffled units. Values of p_r close to zero indicate an ordered arrangement of lithofacies unit thickness that is unlikely to occur by chance.

Results of facies order analysis are consistent with planform statistics showing presence or absence of evidence for order in each model case (Table 2). Case 1 has p_m and p_r values close to 1.0 indicating disordered strata in the vertical section, consistent with the narrow planform subtidal zones and a lack of planform spatial self-organization. In model Cases 2 to 8, p_m values are all <0.1, suggesting ordered and cyclical lithofacies successions generated by organized planform facies patterns. In contrast, the vertical section from Case 9 also has a p_m value of 0.54, providing no evidence of vertical lithofacies order, consistent with the lack of spatial order in planform.

Analyzing facies unit thicknesses, only Case 2 shows strong evidence for ordered thickness trends with $p_r = 0$ (Table 2). Cases 3, 4, 6 and 7 all have p_r values between 0.1 and 0.25, indicating only weak evidence of thickness trends. Rapid accretion on the windward side of islands usually deposits thick intertidal and supratidal sediments, while production in subtidal areas is usually more intermittent and produces thinner units. So, a typical asymmetrical shallowing-upward vertical succession has an upward thickening trend. The ordered thickness trend in Case 2 arises from a uniform island progradation rate, but in all other cases, accumulation rates are too spatially variable to generate cyclical thickening or thinning trends.

In summary, quantitative evidence indicates that ordered vertical strata occur in model cases where planform spatial self-organization is present, and not in the non-self-organized cases. This suggests that migration of planform spatial self-organized patterns in this model commonly produces a cyclical arrangement of facies in vertical section, and, in the simplest case but not

Table 2. Lithofacies and thickness ordering analysis for ten selected vertical sections in the centre of the model grid, including an additional vertical section for Case 9.

Case	1	2	3	4	5	6	7	8	9	
Point location				Y = 10 km X = 3 km						Y = 16 km X = 3 km
Total units	84	128	182	236	234	246	324	333	533	778
Total facies	5	7	7	7	7	7	7	5	4	5
Mean thickness	1.285	0.885	0.623	0.505	0.507	0.511	0.348	0.293	0.159	0.132
p_m	0.965	0.002	0.082	0.000	0.000	0.000	0.000	0.000	1.000	0.542
p_r	0.944	0.000	0.223	0.148	0.804	0.125	0.150	1.000	1.000	0.741

The Pm values are very consistent with platform top maps and cross-section, Cases 2 to 8 are all highly ordered with p_m values close to 0, while Case 1 and Case 9 show no evidence of order with much higher p_m values. The p_r value is more sensitive to the disorder, so only Case 2 still shows strong evidence of an ordered thickness trend, Cases 3, 4, 6 and 7 show weak evidence for thickness ordering other cases with high F or K values have no such evidence.

the others, ordered trends in the layer thicknesses.

When might spatial self-organization occur on carbonate platforms?

In model Cases 2 to 8, a mean subtidal zone width >1 km is sufficient to create self-organized dynamic equilibrium patterns of supratidal island formation and progradation. There is also strong evidence for ordered, cyclical facies arrangement in the strata that results from the self-organized island progradation; evidence for cyclicity is then by extension, in this case at least, evidence for self-organization. However, these model cases are only a small sample of the range of carbonate production and sediment transport rate values that could realistically occur on a carbonate platform top, so it is important to determine where self-organization occurs in a broader range of the whole model parameter space.

A total of 400 model runs were executed and analyzed to map the occurrence of self-organization in a broad parameter space with production rates from 0 to 400 m/Myr, and sediment transport fractions from 0.0 to 1.0. Aside from different production and transport rates, all of the model runs were formulated in the same way as Case 7.

Parameter space plots show that mean subtidal zone width and the Markov order p_m vary quite smoothly across the parameter space in response to varying sediment production and transport rates (Fig. 6A and B). Evidence from these two indicators shows where self-organization occurs in models in the parameter space (Fig. 6C). With the given subsidence rate and initial topography, onshore sediment flux is limited to a certain range to satisfy the A/S ratio requirement. Models with subtidal zone widths >1 km and strong statistical evidence for ordered, cyclical strata occur when the production rate is between 100 and 250 m/Myr, and transport fraction is between 0.25 and 1.0, with a broader range of production rates producing self-organized strata when the transport fraction is higher. This distribution of self-organization within the parameter space is consistent with explanations above of how self-organization occurs; when the subtidal zone is wide enough to supply sufficient sediment to the landward shoreline to ensure an A/S ratio of approximately one, self-organized island progradation and cycle formation occur. In other areas of the parameter space (blue in Fig. 6C) either island progradation is too disorganized to create cycles, or no island progradation occurs. This threshold subtidal factory width of 1 km in the model is the minimum width required to produce sediment and drive shoreline progradation against subsidence, and it can be viewed as a criticality behaviour in a self-organized system, which is essentially a specific form of divergence with sudden shifts across a threshold (Fagherazzi, 2008; Plotnick, 2016; Purkis *et al.*, 2016b). Importantly, this plot suggests that for any carbonate platform top system with cross-platform sediment

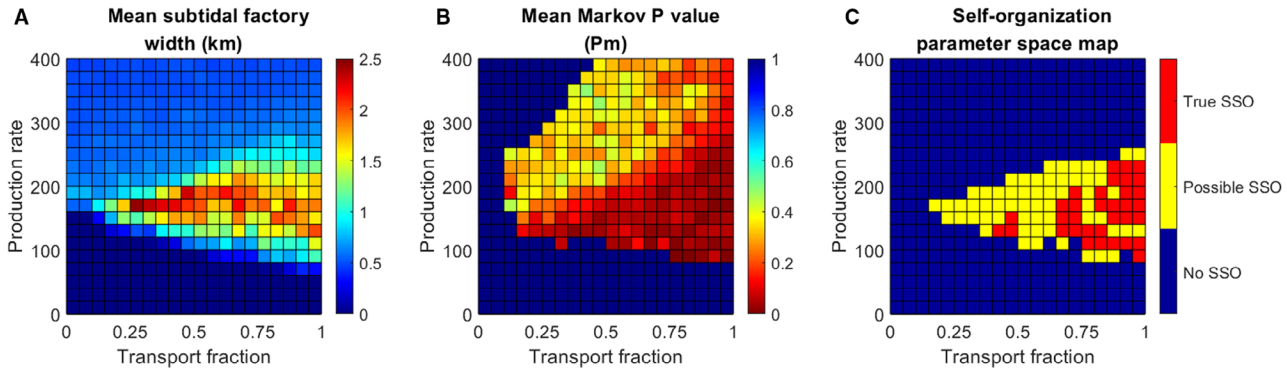

Fig. 6. (A) Parameter space plot of input production rate and transport fraction for 400 model runs, colour coded according to the mean subtidal zone width *Ws*. (B) The same parameter space, but colour coded with the vertical facies order metric, p_m. (C) With the same parameter space colour coded to show a logical combination of evidence for self-organization from (A) and (B) such that blue indicates model runs in which $Ws < 1$ km and $p_m > 0.05$, yellow is either $Ws > 1$ km or $p_m < 0.05$, but not both, so weak evidence for self-organization, and red is $Ws > 1$ km and $p_m < 0.05$ so strong evidence for self-organization. From this, it is clear that self-organized models, with strongly developed autocycles, are restricted in this case to a specific range of A/S ratios, given the constant rate of subsidence in this model, consistent with explanations above of how self-organization occurs in the model.

transport, and without high-amplitude high-frequency external eustatic forcing, if production and transport rates both fall within a certain range, coherent patterns of island morphologies and ordered cyclic strata are likely to occur due to the self-organizing interactions between subsidence, production, transport and topography.

COMPARISON WITH MODERN AND ANCIENT CARBONATE SYSTEMS

Shoreline progradation in modern carbonate systems

Carbonate sequence stratigraphic models have tended to focus on accommodation as the dominant control on long-term deposition and stacking patterns (Goldhammer *et al.*, 1987, 1990; Chen *et al.*, 2001; Bosence *et al.*, 2009). Here however the focus is on a more complex combination of processes controlling stacking patterns, the most important being sediment transport onto a shoreline driving shoreline progradation, as first suggested by Ginsburg (1971). These modelling results suggest that if sediment is transported from a subtidal zone onto a shoreline and can drive shoreline progradation, there is potential for the self-organizing process modelled here to occur, even if in more varied and complex forms than these simple models show. For this reason, it is important to demonstrate that basic aspects of shoreline progradation at similar rates does occur on modern carbonate platforms, to establish that this numerical model is realistic at least in terms of the basic underlying process driving the more complex behaviour.

Model results are compared to observations from a modern carbonate atoll, Peros Banhos, located in the British Indian Ocean Territory, where good data exist showing platform top

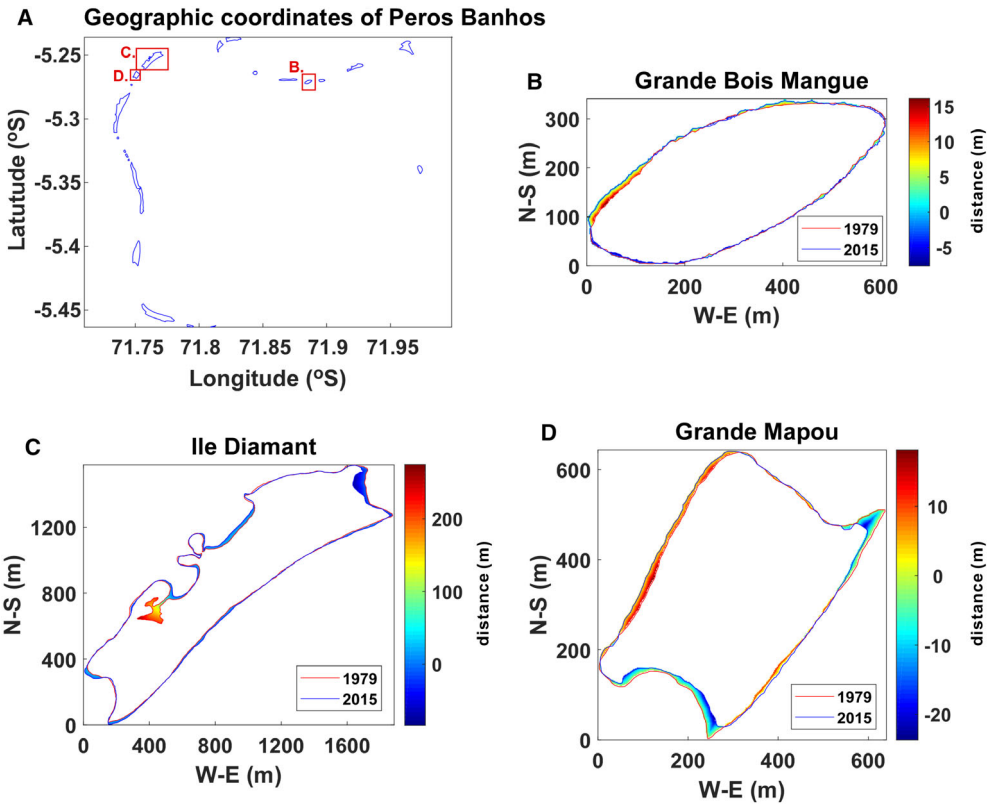

Fig. 7. (A) Location and coastline maps for the islands of Peros Benhos, in the British Indian Ocean Territory. (B) Shoreline progradation (red) of ocean-facing coastline of Grande Bois Mangue, the colour bar represents migration distance (m) from 1979 to 2015. (C) Highest shoreline progradation occurs on the ocean-facing coastline of Ile Diamant, which has an average progradation rate of 1000 m/kyr, local rate can be up to 7220 m/kyr due to rapid infilling of embayment. (D) Shoreline progradation (red) of ocean-facing coastline of Grande Mapou, which is more uniform compared to Ile Diamant. Courtesy of Mingyue Wu and Sam Purkis.

shoreline evolution through time. Shoreline migration rates were measured for a suite of atoll islands from satellite images from 1979 and 2015. In general, ocean-facing coastlines expand and prograde, while the lagoon-facing coastlines retreat [Fig. 7; also see fig. 4 in Wu *et al.* (2021a)]. Calculated rates demonstrate that the ocean-facing coast has an average expansion or progradation rate of 180 m/kyr and an average retreat rate of 340 m/kyr, assuming that these short-term rates will be maintained over geological timescales. The lagoon-facing coast has an average progradation rate of 160 m/kyr, and an average retreating rate of 150 m/kyr (Wu *et al.*, 2021a). The highest rate of shoreline change occurs on the island 'Ile Diamant', which has an average progradation rate of 1000 m/kyr, and locally up to 7220 m/kyr due to rapid filling of a low energy embayment that is subsequently stabilized by terrestrial vegetation (Fig. 7C). This distribution of progradation rates is spatially complex compared to the current model, reflecting more complex platform-top sediment transport routes controlled by topography, waves and currents. Shoreline expansion and retreat are rapid, but also balanced, so the total island area is maintained and stable with −0.004% average areal change (Wu *et al.*, 2021a).

On the nearby Diego Garcia platform, the largest atoll island in the Chagos, shorelines prograde at an average rate of 210 m/kyr (Purkis *et al.*, 2016a) suggesting that rates observed on Peros Banhos are not unusual. Similarly, progradation rates of a shoreline in Abu Dhabi, on the low-angle carbonate ramp in the southern shore of the Persian Gulf, derived from radiocarbon dating yield a range between 340 to 1030 m/kyr (Lokier & Steuber, 2008). The south-west Andros Island tidal flats also share some similar characteristics with the initial conditions, sedimentary processes and products that are modelled in this study. Carbonate-producing subtidal zones are <1 m deep at low tide, and there is no appreciable bathymetric gradient. Continued landward transport of carbonate muds has developed a spatially complex patchwork pattern of subtidal, intertidal and supratidal sediment penetrated by a few broad tidal channels (Rankey & Berkeley, 2012). The south-west-facing shoreline has prograded at an even higher rate between 5 to 20 km/kyr since the Holocene transgression (Handford & Loucks, 1993), and preserved shoreline relicts suggest that progradation occurred in a series of pulses rather than continuous accretion at the shoreface (Gebelein, 1974; Rankey & Berkeley, 2012).

Florida Bay is another good modern example, characterized by a series of shallow subtidal lagoons, intertidal mud banks and supratidal islands (Enos & Perkins, 1979). The central bay, in particular, contains about 150 sinuous mud banks with islands that preferentially nucleate on the windward bank edges, stabilized by mangrove trees (Enos, 1989). These islands are dynamic and can migrate due to erosion, lateral accretion and merging of islands, but their areas in planform and volumes remain constant (Enos, 1989), indicating a possible state of dynamic equilibrium.

In comparison to the various observations above, the average shoreline progradation rate in the current model is 110 m/kyr. So the modelled progradation rates seem reasonable based on these data from Wu *et al.* (2021a), with the important caveat that there is some uncertainty in this rate match because this model has a total elapsed time of 2 Myr, much longer than interval of observation on modern platform tops. Nevertheless, these observation data from a modern carbonate system validate the progradation rates modelled here, suggesting that shoreline progradation creating upward-shallowing autocycles is possible on several modern carbonate platforms, and therefore likely to be ubiquitous in the stratigraphic record.

This raises the question: if shoreline and island progradation does happen, why do we not more commonly see well-developed patterns of prograding islands separated by subtidal areas, as the model predicts, on modern carbonate platforms? The reason is most likely that modern carbonate platform tops have been recently reflooded during the rapid Holocene glacio-eustatic sea-level rise, with rates of approximately 1 mm/year over the past 5 to 6 kyr (Miller *et al.*, 2005). Shoreline progradation is unlikely to keep up with such rapid rates of relative sea-level rise, and well-developed progradational island systems will take time to reform after such rapid flooding. For example, the seaward margin of north-west Andros tidal flats in Great Bahama Bank shows no progradation but aggraded and locally retrograded (Shinn *et al.*, 1969; Hardie, 1977; Rankey & Morgan, 2002), in response to a 10 cm rise of sea-level from 1943 to 2018 (Wu *et al.*, 2021b). However, such high-frequency and high-amplitude eustatic oscillations are relatively rare in geological history, representing <25% of Phanerozoic time (e.g. Scotese *et al.*, 2021). Therefore, it seems plausible that ancient carbonate platforms, formed in warmer climate intervals

with smaller terrestrial ice sheets, probably featured extensive progradational islands, shorelines and autocycles of the type modelled here. If so, self-organized upward-shallowing autocycles are likely to be common in the stratigraphic record. A useful next step could be to apply this kind of modelling analysis to explore the history and potential future evolution of the Florida Bay islands and the south-west Andros coastline system, to understand what kind of vertical succession of strata is likely to be produced in the long-term in those two systems.

Significance for outcrop and subsurface interpretation

If carbonate platform strata were only controlled by relative sea-level oscillations, they should be synchronous and laterally persistent across the entire platform (Goodwin & Anderson, 1985; Read & Goldhammer, 1988), or even between basins (Osleger & Read, 1991). Yet many peritidal carbonate strata deposited in a greenhouse setting are characterized by complex cycle patterns with rapid lateral facies change and pronounced lateral thickness variation (Pratt & James, 1986; Bosence *et al.*, 2009; Pratt, 2010; Christ *et al.*, 2012; Sena & John, 2013; Yang *et al.*, 2014; Samankassou & Enos, 2019) that preclude a simple allogenic forcing model and point to the possibility of more complex autogenic processes.

Pratt & James (1986) documented rapid lateral facies changes and limited correlation between two vertical peritidal sections of the Lower Ordovician St George Group in western Newfoundland, located 2 km apart. Subaerial exposure associated facies rarely occur or only occur locally, and the commonest members are alternating subtidal–intertidal beds that lack clear evidence of water depth trend to support an allogenic model. The entire St George Group records a long-term systematic change in facies proportion, only the intervening Catoche Formation is subtidal-dominated, and the other two units both exhibit extensive peritidal strata (Pratt & James, 1986). Given the lack of strong evidence for allogenic forcing and based on the modelling results, the change in facies proportion of these three stratigraphic units can also be explained by difference in the A/S ratio. If the A/S ratio is high either due to insufficient sediment supply or rapid subsidence, islands are only sparsely developed on the platform top, so strata are dominated by subtidal facies. In contrast, when sedimentation outpaces subsidence, supratidal islands and intertidal banks are laterally amalgamated so peritidal cycles can be recorded more completely.

Similar complexity is also observed in the Triassic Dachstein platform (Samankassou & Enos, 2019). Beds are laterally discontinuous even at a scale of 2 km, the overall mean bed thickness variation is 49% due to lateral pinch-out and erosion-associated facies amalgamation. According to their interpretations, such complex stratal stacking patterns are products of spatially variable sediment production and transport, similar to what is modelled here. They also highlight erosion as an important process that can add some additional complexities to this autogenic island progradation process and the resultant stratal stacking patterns, by removing cycles or parts of cycles, and resulting in non-Waltherian facies contacts. For example, tidal channels can cut through islands and weaken the influence of island topography as 'barriers' by accumulating muds in its lee (Maloof & Grotzinger, 2012; Wu *et al.*, 2021b). Storm event associated erosion or deposition can significantly modify island morphology in a very short time (Wanless, 1979), adding lateral variability to shoreline expression and morphology (Rankey & Morgan, 2002). If these erosional surfaces are not properly detected and located, interpreting water depth trends and cycles can lead to problematic facies correlation, as highlighted in some previous models (Burgess & Wright, 2003).

Many ancient examples share similarities with this modelling in the interpreted dynamic behaviours of tidal flat islands as they migrate laterally and accrete vertically to deposit metre-scale peritidal cycles. Since they all contain a significant portion of strata that lack definitive evidence of relative sea-level fluctuations (for example, abnormal subaerial exposure, abrupt platform margin facies downstepping), it is perhaps necessary to move to a more balanced approach in which autogenic processes have equal weight in interpretations alongside allogenic processes.

DISCUSSION

Spatial self-organization is a process in physical, chemical and biological systems in which spatially complex patterns can arise from local interactions of individual system components in a system with emergent properties and threshold

behaviours to produce patterns that are not forced by any external input to the system (Plotnick, 2016). Self-organization processes are pervasive and widely documented across many natural systems (Rietkerk & Koppel, 2008; Hajek *et al.*, 2010; Paola, 2016). Yet, as Purkis *et al.* (2016b) points out: "at the moment, spatial self-organization in carbonate systems is an intriguing hypothesis more than an established fact".

Some examples of self-organization in modern carbonate depositional systems are documented, but what is often unclear is how the self-organization is preserved as strata in the geological record. Rankey & Reeder (2011) showed a potentially self-organized, autogenic example from a Holocene oolitic shoal system in the Bahamas, in which ordered geomorphological patterns emerge from spatial interaction and feedback between topography, hydrodynamics, sediment production and transport across multiple scales, from individual bedforms, to geomorphic bar forms and the entire shoal complexes, with clear links between two successive scales. Each ooid shoal is unique in detail, strongly coupled with those formative processes and constrained by the larger-scale boundary conditions (Rankey & Reeder, 2011). This is similar and comparable to the platform-top island spatial distribution that emerges in this model as a dynamic equilibrium pattern conditioned by the regional subsidence rate and sediment flux. Each island has a different morphology controlled by the corresponding A/S ratio at each prograding island shoreline, ultimately determined by the complex spatial feedbacks between topography, sediment production and transport. van de Vijsel *et al.* (2019) integrated field and laboratory study from the Schelde estuary, Netherlands, and showed that present day microbial mats can self-organize and develop regular metre-scale mat-covered ridges and bare runnels on intertidal flats, due to scale-dependent interactions between biofilm stabilization, runnel erosion, sediment transport and hydrodynamics. These modern organo-sedimentary deposits are strikingly similar to microbialite strata found in the geological record, in their internal laminations, biological functions and morphological patterns, suggesting that the existence and possible significance of self-organization in carbonate strata can be traced back to the Proterozoic.

An important aspect of the numerical forward modelling is that it demonstrates how a self-organized geomorphic pattern can be preserved as a pattern in the vertical accumulation of strata. Prograding self-organized islands create cyclical strata with strong statistical evidence, showing how a transient geomorphic pattern can be translated into a deep-time stratigraphic pattern. Preservation of self-organized geomorphic patterns as stratigraphic patterns is particularly important to understand in carbonate stratigraphy because when cyclicity is observed in carbonate strata it is most often interpreted as a consequence of forcing by a dominant external control, most often relative sea-level oscillations that control accommodation (Goldhammer *et al.*, 1987, 1990; Chen *et al.*, 2001). Part of the reason for this assumed dominance of external sea-level forcing to create cyclicity is the assumption that autogenic processes add noise to strata, not a signal, and if they do create a signal, the signal is often assumed to be on a local scale and of short duration (Lehrmann & Goldhammer, 1999). The results from this model challenge this simple assumption, showing that autogenic island and shoreline progradation, as observed to happen on modern carbonate platforms, can also create vertically-ordered strata with strong cyclicity with a time span of 10^5 to 10^6 years, and either laterally discontinuous or laterally continuous over scales of 10^3 to 10^4 metres, depending on the actual interaction between system components in the system. Both cyclicity and lateral continuity of facies are determined not simply by the level of autocyclicity, but are sensitive to planform progradation rate, which is in turn sensitive to the spatial variability of sediment production and transport.

However, many ancient carbonate successions in outcrop do not develop the strong cyclicity developed in these model results. Instead, many carbonate platform strata, when observed carefully in outcrop and especially when analyzed using robust quantitative methods, are more complex and noisier (Wilkinson *et al.*, 1999; Bosence *et al.*, 2009; Burgess, 2016). The complexity and noise may arise from processes such as tidal channel migration, storm erosion, slope instability, tsunami backwash and various biological activities, that are not modelled here, but can make strata effectively indistinguishable from random successions (Wanless, 1981; Cloyd *et al.*, 1990; Peper & Cloetingh, 1995; Bosence *et al.*, 2009; Samankassou & Enos, 2019; Pratt & Rule, 2021). Nevertheless, whenever strong evidence for ordered strata with only weak or no evidence for relative sea-level forcing [for example, abnormal subaerial exposure of subtidal strata, see Lehrmann & Goldhammer (1999)], autogenic cyclicity

due to self-organization should always be considered as a possible explanation.

Finally, further work is definitely required, to help understand exactly how such self-organization works on carbonate platforms that are also forced by external controls such as relative sea-level and climate oscillations, as well as influenced by short term 'noisy' events and intrinsic complexity of multiple interacting processes. Quantitative analysis of spatial patterns and gap size can provide useful insights to characterize facies distribution and the fractal nature of patch size (Plotnick *et al.*, 1993; Rankey, 2002). As ever, the best approach to this is a careful mix of experimental numerical modelling, combined with and constrained by analysis of and comparison with modern and ancient carbonate systems, all focused on addressing the complexity observed in this study, rather than assuming a false simplicity that probably exists only in sequence stratigraphic conceptual models.

CONCLUSION

Results from this modelling study suggest several significant conclusions:

1 Shallowing-upward carbonate peritidal autocycles can form due to self-organizing interactions between carbonate sediment production, sediment transport and accommodation creation, without any allogenic forcing. The simplest possible model formulation producing self-organization includes only water-depth-dependent production, simple cross-platform sediment transport and uniform subsidence.

2 Subtidal zone width determines the sediment production and supply to the adjacent island, which in turn determines the island progradation rate and the resulting autocycle thickness. As shorelines and islands prograde, they arrange themselves to form a predictable pattern of planform island spacing such that subtidal zone width is just enough to drive progradation with an accommodation creation/sediment supply (A/S) ratio of around one, which is indicative of the degree of spatial self-organization. This happens in model Cases 2 to 8, but not in the other two models because they have either insufficient onshore sediment flux or high rates of local sediment transport.

3 Mapping of self-organization in the model parameter space shows that self-organization can and only occur for a limited range of production and transport rates, where the resulting subtidal width is above a critical value, suggests that self-organization is a specific form of autogenic process.

4 Comparison of the modelled shoreline progradation rate with similar progradation measured from time-lapse satellite imagery on modern carbonate platforms suggests that this process of autocycle formation is realistic, occurs at similar rates to those modelled here, and so maybe commonly recorded in ancient carbonate platform strata. However, other processes, for example relatively rare high-amplitude high-frequency glacioeustatic oscillations might overprint it, as is likely the case for Pleistocene and Holocene platforms. As ever, quantitative analysis and multiple hypotheses in interpretations of ancient strata are key.

5 Cyclothems created by this self-organizing island progradation process could be laterally continuous from the landward shoreline to platform margin, so autogenic processes under some suitable conditions offer a plausible mechanism to create extensive ordered, correlative carbonate platform strata. However, most situations where autogenic processes dominate are likely to create rather more disordered, discontinuous strata due to the complexity of carbonate platform-top processes. A more balanced approach for evaluating allogenic and autogenic processes should be applied when interpreting ancient strata, fully considering both allogenic and autogenic processes.

ACKNOWLEDGEMENTS

We thank Mingyue Wu and Sam Purkis for providing aerial photography; and Gene Rankey and Brian Pratt for providing very helpful suggestions and comments on the manuscript.

DATA AVAILABILITY STATEMENT

The data that support the findings of this study are available from the corresponding author upon reasonable request.

REFERENCES

Bosence, D., **Procter, E.**, **Aurell, M.**, **Bel Kahla, A.**, **Boudagher-Fadel, M.**, **Casaglia, F.**, **Cirilli, S.**, **Mehdie, M.**, **Nieto, L.**, **Rey, J.**, **Scherreiks, R.**, **Soussi, M.** and **Waltham, D.** (2009) A dominant tectonic signal in high-frequency, peritidal carbonate cycles? A regional analysis of Liassic

platforms from Western Tethys. *J. Sediment. Res.*, **79**, 389–415.

Bosscher, H. and **Schlager, W.** (1992) Computer simulation of reef growth. *Sedimentology*, **39**, 503–512.

Budd, D.A., **Hajek, E.A.** and **Purkis, S.J.** (2016) Introduction to autogenic dynamics and self-organization in sedimentary systems. In: *Autogenic Dynamics and Self-Organization in Sedimentary Systems* (Eds Budd, D.A., Hajek, E.A. and Purkis, S.J.), *SEPM Special Publication*, **106**, 1–4.

Burgess, P.M. (2001) Modeling carbonate sequence development without relative sea-level oscillations. *Geology*, **29**, 1127–1130.

Burgess, P.M. (2006) The signal and the noise: Forward modeling of allocyclic and autocyclic processes influencing peritidal carbonate stacking patterns. *J. Sediment. Res.*, **76**, 962–977.

Burgess, P.M. (2013) CarboCAT; a cellular automata model of heterogeneous carbonate strata. *Comput. Geosci.*, **53**, 129–140.

Burgess, P.M. (2016) Identifying Ordered Strata: Evidence, Methods, and Meaning. *J. Sediment. Res.*, **86**, 148–167.

Burgess, P.M., **Wright, V.P.** and **Emery, D.** (2001) Numerical forward modelling of peritidal carbonate parasequence development: implications for outcrop interpretation. *Basin Res.*, **13**, 1–16.

Burgess, P.M. and **Wright, V.P.** (2003) Numerical forward modeling of carbonate platform dynamics; an evaluation of complexity and completeness in carbonate strata. *J. Sediment. Res.*, **73**, 637–652.

Chen, D., **Tucker, M.E.**, **Jiang, M.** and **Zhu, J.** (2001) Long-distance correlation between tectonic-controlled, isolated carbonate platforms by cyclostratigraphy and sequence stratigraphy in the devonian of South China. *Sedimentology*, **48**, 57–78.

Christ, N., **Immenhauser, A.**, **Amour, F.**, **Mutti, M.**, **Preston, R.**, **Whitaker, F.F.**, **Peterhänsel, A.**, **Egenhoff, S.O.**, **Dunn, P.A.** and **Agar, S.M.** (2012) Triassic Latemar cycle tops — Subaerial exposure of platform carbonates under tropical arid climate. *Sed. Geol.*, **265–266**, 1–29.

Cloyd, K.C., **Demicco, R.V.** and **Spencer, R.J.** (1990) Tidal channel, levee, and crevasse-splay deposits from a Cambrian tidal channel system; a new mechanism to produce shallowing-upward sequences. *J. Sediment. Res.*, **60**, 73–83.

Crank, J. (1975) *The Mathmatics of Diffusion*, 2nd edn. Claredon Press, Oxford.

Davis, J.C. (2002) *Statistics and Data Analysis in Geology*, 3rd edn. New York: John Wiley and Sons, 638 pp.

Drummond, C.N. and **Dugan, P.J.** (1999) Self-organizing models of shallow-water carbonate accumulation. *J. Sediment. Res.*, **69**, 939–946.

Drummond, C.N. and **Wilkinson, B.H.** (1993) Aperiodic accumulation of cyclic peritidal carbonate. *Geology*, **21**, 1023–1026.

Enos, P. (1989) Islands in the Bay—a key habitat of Florida Bay. *Bull. Mar. Sci.*, **44**, 365–386.

Enos, P. (1991) Sedimentary parameters for computer modeling. *Kansas Geol. Surv. Bull.*, **233**, 63–99.

Enos, P. and **Perkins, R.D.** (1979) Evolution of Florida Bay from island stratigraphy. *GSA Bulletin*, **90**, 59–83.

Fagherazzi, S. (2008) Self-organization of tidal deltas. *Proc. Natl Acad. Sci. USA*, **105**, 18692–18695.

Fedele, J.J., **Hoyal, D.**, **Barnaal, Z.**, **Tulenko, J.** and **Awalt, S.** (2016) Bedforms created by gravity flows. In: *Autogenic Dynamics and Self-Organization in Sedimentary Systems* (Eds Budd, D.A., Hajek, E.A. and Purkis, S.), *SEPM Society for Sedimentary Geology*, **106**.

Gebelein, C.D. (1974) *Guidebook for Modern Bahamian Platform Environments*: Geological Society of America annual meeting field trip guide.

Ginsburg, R.N. (1971) Landward movement of carbonate mud–new model for regressive cycles in carbonates (abs.). *Am. Assoc. Petrol. Geol.*, **55**, 340.

Goldhammer, R.K., **Dunn, P.A.** and **Hardie, L.A.** (1987) High frequency glacio-eustatic sealevel oscillations with Milankovitch characteristics recorded in Middle Triassic platform carbonates in northern Italy. *Am. J. Sci.*, **287**(9), 853–892.

Goldhammer, R.K., **Dunn, P.A.** and **Hardie, L.A.** (1990) Depositional cycles, composite sea-level changes, cycle stacking patterns, and the hierarchy of stratigraphic forcing: Examples from Alpine Triassic platform carbonates. *GSA Bulletin*, **102**, 535–562.

Goldhammer, R.K., **Lehmann, P.J.** and **Dunn, P.A.** (1993) The origin of high-frequency platform carbonate cycles and third-order sequences (Lower Ordovician El Paso Gp, West Texas); constraints from outcrop data and stratigraphic modeling. *J. Sediment. Res.*, **63**, 318–359.

Goodwin, P.W. and **Anderson, E.J.** (1985) Punctuated aggradational cycles: A general hypothesis of episodic stratigraphic accumulation. *J. Geol.*, **93**, 515–533.

Hajek, E.A., **Heller, P.L.** and **Sheets, B.A.** (2010) Significance of channel-belt clustering in alluvial basins. *Geology*, **38**, 535–538.

Handford, C.R. and **Loucks, R.G.** (1993) Carbonate depositional sequences and systems tracts—responses of carbonate platforms to relative sea-level changes. In: *Carbonate Sequence Stratigraphy: Recent Developments and Applications*, Vol. **57** (Eds Loucks, R.G. and Sarg, J.F.), pp. 1–39. American Association of Petroleum Geologists, Plano, Texas, USA.

von Hardenberg, J., **Meron, E.**, **Shachak, M.** and **Zarmi, Y.** (2001) Diversity of vegetation patterns and desertification. *Phys. Rev. Lett.*, **87**, 198101.

Hardie, L.A. (1977) *Sedimentation on the Modern Carbonate Tidal Flats of Northwest Andros Island, Bahamas*, Vol. **22** (Ed. Hardie, L.). The Johns Hopkins University Press, Baltimore, 202 pp.

Kaufman, P., **Grotzinger, J.P.** and **McCormick, D.S.** (1991) Depth-dependent diffusion algorithm for simulation of sedimentation in shallow marine depositional systems. *Bull. Kansas Geol. Survey*, **233**, 489–508.

Kenyon, P.M. and **Turcotte, D.L.** (1985) Morphology of a delta prograding by bulk sediment transport. *GSA Bull.*, **96**, 1457–1465.

Kim, W., **Petter, A.L.**, **Straub, K.** and **Mohrig, D.** (2014) Investigating the autogenic process response to allogenic forcing. In: *From depositional systems to sedimentary successions on the Norwegian Continental Margin* (Eds Martinius, A.W., Ravnas, R., Howell, J.A., Steel, R.J. and Wonham, J.P.), pp. 127–138. Wiley-Blackwell, West Sussex, UK.

Kocurek, G. and **Ewing, R.C.** (2016) Trickle-down and trickle-up boundary conditions in eolian dune-field pattern formation. In: *Autogenic Dynamics and Self-Organization in Sedimentary Systems* (Eds Budd, D.A., Hajek, E.A. and Purkis, S.J.), *SEPM Society for Sedimentary Geology*, **106**, 18–39.

Lehrmann, D.J. and **Goldhammer, R.K.** (1999) Secular variation in parasequence and facies stacking patterns of platform carbonates: A guide to application of stacking-patterns analysis in strata of diverse ages and settings. In: *Advances in Carbonate Sequence Stratigraphy: Application to Reservoirs, Outcrops and Models*. (Ed Harris, P.M.), *SEPM Society for Sedimentary Geology*, **63**, 187–225.

Levin, S.A. and **Segel, L.A.** (1985) Pattern generation in space and aspect. *SIAM Rev.*, **27**(1), 45–67.

Liu, Q., **Doelman, A.**, **Rottschäfer, V.**, **de Jager, M.**, **Herman, P.M.J.**, **Rietkerk, M.** and **van de Koppel, J.** (2013) Phase separation explains a new class of self-organized spatial patterns in ecological systems. *Proc. Nat. Acad. Sci.*, **110** (29), 11905–11910.

Lokier, S. and **Steuber, T.** (2008) Quantification of carbonate-ramp sedimentation and progradation rates for the Late Holocene Abu Dhabi shoreline. *J. Sediment. Res.*, **78**, 423–431.

Maloof, A.C. and **Grotzinger, J.P.** (2012) The Holocene shallowing-upward parasequence of north-west Andros Island. *Bahamas*, **59**, 1375–1407.

Martinez, P.A. and **Harbaugh, J.W.** (1989) Computer simulation of wave and fluvial-dominated nearshore environments. In: *Elsevier Oceanography Series*, Vol. **49**. (Eds Lakhan, V.C. and Trenhaile, A.S.), pp. 297–340. Elsevier, Radarweg.

Masiero, I., **Kozlowski, E.**, **Antonatos, G.**, **Xi, H.** and **Burgess, P.** (2020) Numerical stratigraphic forward models as conceptual knowledge repositories and experimental tools: An example using a new enhanced version of CarboCAT. *Comput. Geosci.*, **138**, 104453.

Miller, K.G., **Kominz, M.A.**, **Browning, J.V.**, **Wright, J.D.**, **Mountain, G.S.**, **Katz, M.E.**, **Sugarman, P.J.**, **Cramer, B.S.**, **Christie-Blick, N.** and **Pekar, S.F.** (2005) The phanerozoic record of global sea-level change. *Science*, **310**(5752), 1293–1298.

Olivito, J.P.R. and **Souza, F.J.** (2020) Depositional model of early Cretaceous lacustrine carbonate reservoirs of the Coqueiros formation - Northern Campos Basin, southeastern Brazil. *Mar. Pet. Geol.*, **111**, 414–439.

Olszewski, T.D. (2016) Biological self-organization: Implications for sedimentary rocks with examples from shallow marine settings. In: *Autogenic Dynamics and Self-Organization in Sedimentary Systems* (Eds Budd, D.A., Hajek, E.A. and Purkis, S.J.), *SEPM Society for Sedimentary Geology*, **106**, 40–52.

Osleger, D. and **Read, J.F.** (1991) Relation of eustasy to stacking patterns of meter-scale carbonate cycles, Late Cambrian, U.S.A. *J. Sediment. Res.*, **61**, 1225–1252.

Paola, C. (2016) A mind of their own: Recent advances in autogenic dynamics in rivers and deltas. In: *Autogenic Dynamics and Self-Organization in Sedimentary Systems* (Eds Budd, D.A., Hajek, E.A. and Purkis, S.J.), *SEPM Society for Sedimentary Geology*, **106**, 5–17.

Paola, C., **Straub, K.**, **Mohrig, D.** and **Reinhardt, L.** (2009) The "unreasonable effectiveness" of stratigraphic and geomorphic experiments. *Earth Sci. Rev.*, **97**, 1–43.

Peper, T. and **Cloetingh, S.** (1995) Autocyclic perturbations of orbitally forced signals in the sedimentary record. *Geology*, **23**, 937–940.

Petroff, A.P., **Sim, M.S.**, **Maslov, A.**, **Krupenin, M.**, **Rothman, D.H.** and **Bosak, T.** (2010) Biophysical basis for the geometry of conical stromatolites. *Proc. Nat. Acad. Sci.*, **107**, 9956–9961.

Plotnick, R.E. (2016) Lattice models in ecology, paleontology, and geology. In: *Autogenic Dynamics and Self-Organization in Sedimentary Systems* (Eds Budd, D.A., Hajek, E.A. and Purkis, S.J.), *SEPM Society for Sedimentary Geology*, **106**, 83–94.

Plotnick, R.E., **Gardner, R.H.** and **O'Neill, R.V.** (1993) Lacunarity indices as measures of landscape texture. *Landscape Ecol.*, **8**, 201–211.

Pratt, B.R. (2010) Peritidal carbonates. In: *Facies Models 4* (Eds James, N.P. and Dalrymple, R.W.), pp. 401–420. Geological Association of Canada, Toronto.

Pratt, B.R. and **James, N.P.** (1986) The St George Group (Lower Ordovician) of western Newfoundland: tidal flat island model for carbonate sedimentation in shallow epeiric seas. *Sedimentology*, **33**, 313–343.

Pratt, B.R. and **Rule, R.G.** (2021) A Mesoproterozoic carbonate platform (lower Belt Supergroup of western North America): Sediments, facies, tides, tsunamis and earthquakes in a tectonically active intracratonic basin. *Earth Sci. Rev.*, **217**, 103626.

Purkis, S.J., **Gardiner, R.**, **Johnston, M.W.** and **Sheppard, C.R.C.** (2016a) A half-century of coastline change in Diego Garcia – The largest atoll island in the Chagos. *Geomorphology*, **261**, 282–298.

Purkis, S.J., **Koppel, J.V.D.** and **Burgess, P.M.** (2016b) Spatial self-organization in carbonate depositional environments. In: *Autogenic Dynamics and Self-Organization in Sedimentary Systems* (Eds Budd, D.A., Hajek, E.A. and Purkis, S.J.), *SEPM Society for Sedimentary Geology*, **106**, 53–66.

Rankey, E.C. (2002) Spatial patterns of sediment accumulation on a Holocene carbonate tidal flat, Northwest Andros Island, Bahamas. *J. Sediment. Res.*, **72**, 591–601.

Rankey, E.C. and **Berkeley, A.** (2012) Holocene carbonate tidal flats. In: *Principles of Tidal Sedimentology* (Eds Davis R.A. and Dalrymple, R.W.), pp. 507–535. Springer, Dordrecht.

Rankey, E.C. and **Morgan, J.** (2002) Quantified rates of geomorphic change on a modern carbonate tidal flat, Bahamas. *Geology*, **30**, 583–586.

Rankey, E.C. and **Reeder, S.L.** (2011) Holocene oolitic marine sand complexes of the Bahamas. *J. Sediment. Res.*, **81**, 97–117.

Read, J.F. and **Goldhammer, R.K.** (1988) Use of fischer plots to define third-order sea-level curves in Ordovician peritidal cyclic carbonates, Appalachians. *Geology*, **16**, 895–899.

Read, J.F., **Grotzinger, J.P.**, **Bova, J.A.** and **Koerschner, W.F.** (1986) Models for generation of carbonate cycles. *Geology*, **14**, 107–110.

Rietkerk, M. and **van de Koppel, J.** (2008) Regular pattern formation in real ecosystems. *Trends Ecol. Evol.*, **23**, 169–175.

Samankassou, E. and **Enos, P.** (2019) Lateral facies variations in the Triassic Dachstein platform: A challenge for cyclostratigraphy. *Deposit. Rec.*, **5**, 469–485.

Scotese, C., **Song, H.**, **Mills, B.** and **van der Meer, D.** (2021) Phanerozoic paleotemperatures: The Earth's changing climate during the last 540 million years. *Earth Sci. Rev.*, **215**, 103503.

Sena, C.M. and **John, C.M.** (2013) Impact of dynamic sedimentation on facies heterogeneities in Lower Cretaceous peritidal deposits of central east Oman. *Sedimentology*, **60**(5), 1156–1183.

Shinn, E.A., **Lloyd, R.M.** and **Ginsburg, R.N.** (1969) Anatomy of a modern carbonate tidal-flat, Andros island, Bahamas. *J. Sediment. Res.*, **39**, 1202–1228.

Thar, R. and **Kühl, M.** (2005) Complex pattern formation of marine gradient bacteria explained by a simple computer model. *FEMS Microbiol. Lett.*, **246**, 75–79.

Turing, A.M. (1952) The chemical basis of morphogenesis. *Phil. Trans. R. Soc. Lond. B*, **237**, 37–72.

van de Vijsel, R.C., **van Belzen, J.**, **Bouma, T.J.**, **van der Wal, D.**, **Cusseddu, V.**, **Purkis, S.J.**, **Rietkerk, M.** and **van de Koppel, J.** (2019) Estuarine biofilm patterns: Modern analogues for precambrian self-organization. *Earth Surf. Proc. Landf.*, **45**, 1141–1154.

Wanless, H.R. (1979) Role of physical sedimentation in carbonate bank growth. *Am. Asso. Petrol. Geol. Bull.*, **63**, 547.

>Wanless, H.R. (1981) Fining-upwards sedimentary sequences generated in seagrass beds. *J. Sediment. Res.*, **51**, 445–454.

Warrlich, G., **Waltham, D.A.** and **Bosence, D.W.J.** (2002) Quantifying the sequence stratigraphy and drowning mechanisms of atolls using a new 3-D forward stratigraphic modelling program (CARBONATE 3D). *Basin Res.*, **14**, 379–400.

Wilkinson, B.H., **Drummond, C.N.**, **Rothman, E.D.** and **Diedrich, N.W.** (1997) Stratal order in peritidal carbonate sequences. *J. Sediment. Res.*, **67**, 1068–1082.

Wilkinson, B.H., **Drummond, C.N.**, **Diedrich, N.W.** and **Rothman, E.D.** (1999) Poisson processes of carbonate accumulation on Paleozoic and Holocene platforms. *J. Sediment. Res.*, **69**, 338–350.

Williams, H.D., **Burgess, P.M.**, **Wright, V.P.**, **Della Porta, G.** and **Granjeon, D.** (2011) Investigating carbonate platform types; multiple controls and a continuum of geometries. *J. Sediment. Res.*, **81**, 18–37.

Wu, M., **Duvat, V.K.E.** and **Pukis, S.** (2021a) Multi-decadal atoll-island dynamics in the Indian Ocean Chagos Archipelago. *Global Planet. Change*, **202**, 103519.

Wu, M., **Harris, P.**, **Eberli, G.** and **Purkis, S.J.** (2021b) Sea-level, storms, and sedimentation – Controls on the architecture of the Andros tidal flats (Great Bahama Bank). *Sed. Geol.*, **420**, 105932.

Yang, W., **Lehrmann, D.J.** and **Hu, X.-F.** (2014) Peritidal carbonate cycles induced by carbonate productivity variations: A conceptual model for an isolated Early Triassic greenhouse platform in South China. *J. Palaeogeogr.*, **3**, 115–126.

Manuscript received 19 July 2021; revision 6 December 2021; revision accepted 20 December 2021